CHAPTER 4

INVESTIGATIONS OF ADSORPTION BEHAVIOR OF NFCs MODIFIED WITH CATIONIC SURFACTANT; CTAB TOWARDS PHOSPHATE REMOVAL FROM WASTEWATER

4.1 Introduction

This chapter focuses on the synthesis of cationic NFCs and their application in phosphate removal from wastewater. While numerous studies have showcased the efficacy of NFCs in removing various pollutants positively charged cations from wastewaters, there is an urgent need to shift attention towards addressing negatively charged ions as part of the contaminant profile. Exploring NFC's potential for removing anions offers challenging yet promising and cost-effective alternative to the current reliance on other adsorbents for treating wastewater. Furthermore, literature on selective removal of negatively charged ions such as phosphate using NFCs remains scarce, accentuating the need for further investigation in this area [193]. In aqueous solutions, phosphate species carry a negative charge and predominantly exist as $H_2PO_4^-$ at pH levels below 7, which aligns with the typical pH range of wastewater streams.

Surface functionalization of NFCs with quaternary ammonium compounds presents an advantageous approach for the adsorption of negatively charged contaminants [194]. CTAB, a cationic surfactant with long alkyl chain (C16) and a quaternary ammonium head, is particularly known for its hydrophilic-hydrophobic properties, which make it highly versatile in interacting with a wide range of molecules and functional groups [195]. Modifying NFC with quaternary ammonium compounds offers several advantages, particularly the ability to conduct the process in aqueous media [196]. This approach allows for the synthesis of quaternary ammonium compounds in situ, directly

in the presence of NFC, before the reaction proceeds [193,197]. Capron and his team found that the optimal concentration of CTAB reduces the interfacial tension of NFCs, preventing nanoparticle agglomeration and improving dispersion by forming admicelles, where hydrophobic tails point inward toward the core and hydrophilic heads extend outward toward the water phase [198]. Additionally, incorporating CTAB during cationic NFC formation imparts a positive charge to the surface. This positive surface charge facilitates electrostatic interactions between the CTAB-modified NFC and phosphate anions, enhancing phosphate removal from aqueous solutions. Furthermore, the advantages of using CTAB over other compounds include its low cost and extensive availability [199].

Previous research has primarily concentrated on the role of CTAB in the mediated synthesis of nanocomposites with nanocellulose to improve water vapor barrier and mechanical properties, drug delivery systems, tissue engineering systems and water treatment techniques etc. [200–202]. However, the enhanced removal of phosphate using waste-derived NFCs in the presence of CTAB in optimum concentration remains unexplored. Specifically, the underlying removal mechanism, including kinetics and isotherm behaviour, has not been thoroughly studied and warrants detailed investigation. The aim of our investigation are; (i) fabricate cationic NFC using quaternary ammonium surfactant, CTAB; (ii) verify the physico-chemical properties of cationic NFC using sophisticated instrumentation techniques; (iii) evaluate the phosphate removal performance of CTAB-modified NFC using batch removal experiments; (iv) explore the mechanisms underlying phosphate removal by the adsorbent, assess the stability of the adsorbent and its practical applicability through desorption cycles and experiments with interfering anions.

4.2 Synthesis of cationic NFC

The produced NFC from our previous experiments were utilized to synthesize cationic NFC. For synthesis, quaternization modification was carried out using a cationic surfactant; cetyltrimethylammonium bromide. A series of four adsorbents were synthesized with different molar concentration of CTAB (0.5 mM, 1.0 mM, 1.5 mM, and 2.0 mM) to comprehensively evaluate their adsorption performance. Initially, 10 g of NFC was well mixed with 100 mL of 1.5 M NaOH, and kept overnight for stirring at 150 rpm. The next day, CTAB with different molar concentrations aforementioned was added to the suspension and kept for stirring at 50°C for 6 h. Following this, the individual mixture was kept at incubation at ambient temperature for 24 h. The reaction mixture was then neutralized with 1 M HCl and thoroughly washed with deionized water until no free Cl^- ions were detected in the filtrate using $AgNO_3$ solution, followed by filtration. The obtained slurry was then subjected to ultrasonication using digital ultrasonicator (Toshcon India, ultrasonic power supply: 50 Hz, consumption power: 160 W) for 30 minutes for proper disintegration. It was again filtered and kept at drying in oven overnight. Finally, a fine composite powder was obtained by grinding the flakes with a mortar and pestle, resulting in the preparation of CTAB-modified NFC. It was sieved through a mesh (number 100, (≤0.149 mm screen size) and labelled as $CTAB_{0.5}$@NFC, $CTAB_1$@NFC, $CTAB_{1.5}$@NFC $CTAB_2$@NFC (according to molar concentration) for future understanding. Fig. 4.1 denotes the synthesis procedure of CTAB@NFC.

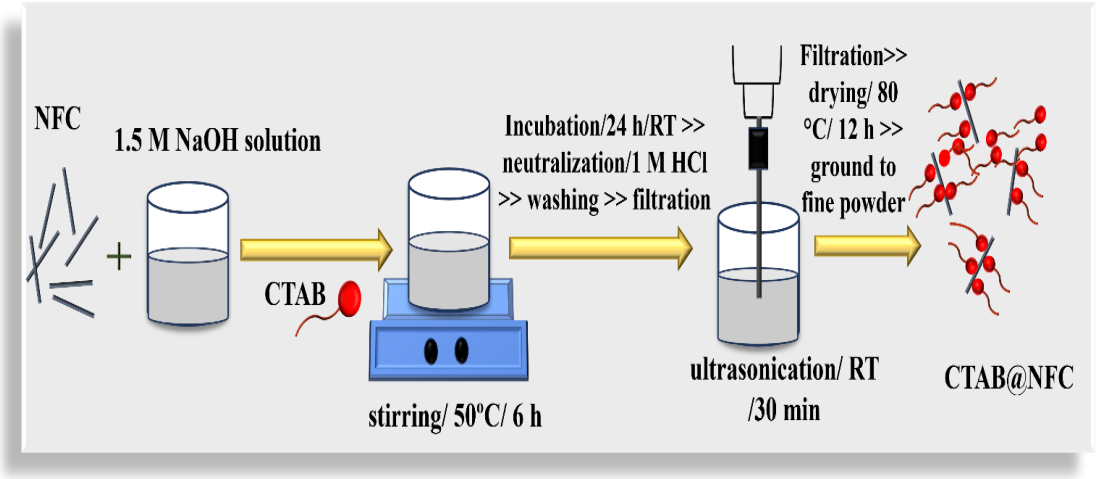

Figure 4.1 Schematic diagram depicting the fabrication process of CTAB@NFC.

4.3 Results and Discussions

4.3.1 Characterization of synthesized adsorbent

4.3.1.1 Scanning Electron Microscopy and Energy-Dispersive X-ray Spectroscopy (SEM-EDS)

SEM analysis was conducted to evaluate the structural and morphological characteristics of NFC and CTAB@NFC adsorbent, both prior to and post adsorption. (Figure 4.2). SEM micrographs illustrate that unmodified NFC exhibits heterogeneity and irregularities, with nanofibrils extending along its axial filament (Figure 4.2 a) [175]. However, following functionalization, the cationic NFC exhibits enhanced unevenness and a more dispersed spatial arrangement due to shape-directing role of CTAB (Figure 4.2 b) [203,204]. This structural transformation is also likely driven by the charges within the cationic NFC, which facilitate disintegration through fibril repulsion leading to greater number of active sites [205,206]. These modifications make the material highly suitable for adsorption process. The BSE image reveals the compositional differences in the sample by detecting variations in the atomic number

[134]. To gain a clearer understanding, we utilized BSE imaging of CTAB@NFC post sorption, which showed substantial changes compared to the surface prior to adsorption (Figure 4.2 c). It was observed that the particles had intercalated over one another and the active sites were occupied by phosphate ions, indicating successful adsorption. Figures 4.3 a and 4.3 b illustrate the distribution spectra of surface elements before and after phosphate adsorption. In the pre-adsorption spectrum, distinct characteristic peaks for nitrogen and bromine are clearly observed that indicates that CTAB surfactant is successfully loaded onto NFC. In the post-adsorption spectrum, a clear and characteristic peak for phosphorus was evident, demonstrating successful phosphate adsorption by the material. From the surface element distribution images indicated in Figure 4.3, post-adsorption distribution of phosphorus was analysed and it relatively revealed a uniform elemental dispersion.

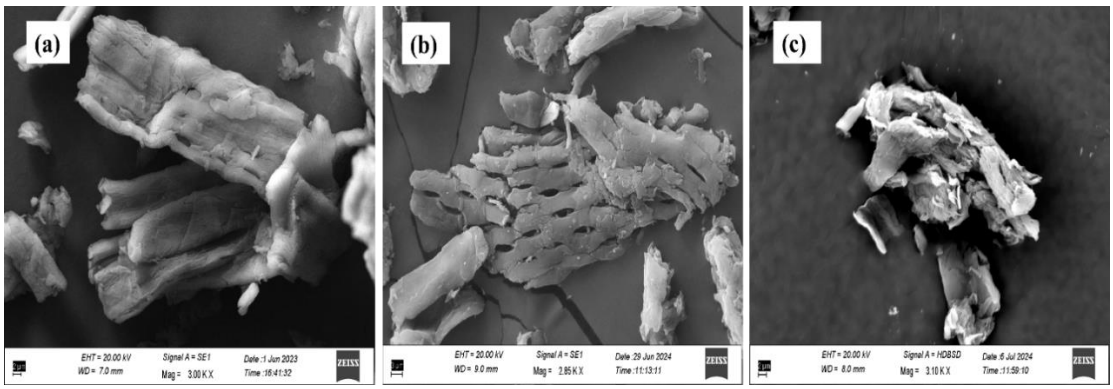

Figure 4.2 SEM images of; (a) pristine NFC; (b) CTAB@NFC (before adsorption); (c) CTAB@NFC*P (after adsorption).

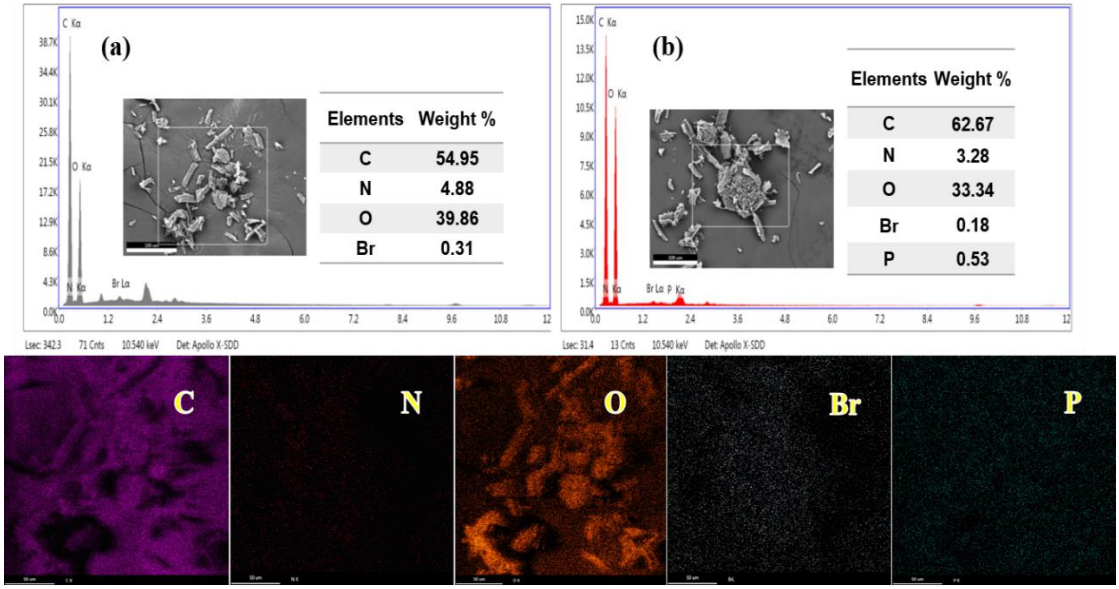

Figure 4.3 EDS spectra and corresponding element distribution content of; (a & b) CTAB@NFC (before and after adsorption) respectively; EDS mapping of C, O, N, Br, P and elemental distribution of CTAB@NFC (after adsorption).

4.3.1.2 Fourier Transform Infrared Spectroscopy (FT-IR)

FT-IR analysis was performed to investigate the functional groups present on the surface of synthesized cationic adsorbent pre-adsorption and post-adsorption, aiming to discern the nature of its interaction with phosphate ions (Figure 4.4 a). FTIR pattern of pristine CTAB and NFC samples are also illustrated in the figure. The FTIR spectrum of pristine CTAB exhibits two prominent bands at 2910 cm^{-1} and 2850 cm^{-1} conforming to asymmetric and symmetric C-H vibrations respectively [207]. Similar bands are also evident in the spectra of CTAB-modified NFC. Additionally, the FTIR spectra of CTAB displays a distinct peak at 1480 cm^{-1}, which is attributed to the asymmetric C-H scissoring vibrations of the trimethyl groups of the quaternary ammonium (CH_3-N^+ moiety) [208]. Furthermore, the peak around 900 cm^{-1} is associated with C-N^+ stretching vibrations, while the characteristic C-Br stretching frequency of cetyltrimethylammonium bromide at 720 cm^{-1}, observed in CTAB and modified samples but not in pristine NFC, further confirms the presence of CTAB on

NFC [209]. It was noted that post sorption, the peaks repositioned to lower wavenumbers and the intensity of the spectrum significantly weakened. Specifically, a minor peak around 1600 cm^{-1} belonging to the bending vibration of the physically adsorbed H_2O disappeared on CTAB@NFC after adsorption. Also, a decreasing trend was observed for the peaks at 3335, 2900, 1490, and 1215 cm^{-1}, which are primarily due to changes in counter ions associated with CTAB modification. This indicates that majority of the surface hydroxyl groups were substituted by adsorbed phosphate. In addition, the spectrum of P-loaded CTAB-modified NFC displayed prominent new peaks at 1125 cm^{-1} and 1050 cm^{-1} which are ascribed to the bending vibration of phosphate, indicating that phosphate had successfully adsorbed onto the surface of the adsorbent [210].

4.3.1.2 X-ray Diffraction (XRD)

The peaks at 14º, 16.4º, 22.2º, and 34º, observed in both NFC and modified NFC as shown in Figure 4.4 b, correspond to the planes (010), (110), (200), and (040) of cellulose I in nanofibrillated celluloses [211]. A marginal decrease in apparent crystallinity index was observed (from 65.5% to 63.1%), which is experimentally semi-quantitative. This reduction is likely a result of the disruption of cellulose crystalline structure and introduction of the substantially long alkyl chain of CTAB, which may enhance the amorphous phase of the material. However, the modification with CTAB did not introduce any new XRD peaks, due to smaller concentrations of CTAB used in modification process, indicates that the overall structure of cellulose remains unaffected [209].

4.3.1.3 BET analysis

N_2 adsorption–desorption analysis was employed to determine the specific surface area and porosity characteristics of CTAB@NFC, with results summarized in Table 4.1 The nitrogen sorption isotherm for the sorbent is presented in Figure 4.4 c. Based on the IUPAC classification, the isotherms with sharp N_2 adsorption at a high relative pressure ($P/P_0 > 0.8$), can be assigned to H3 hysteresis loop and type IV isotherm [212]. The large hysteresis loop type IV suggests a well-defined mesoporous structure with a narrow pore size distribution, providing more accessible active sites and strong adsorbate-adsorbent interactions. The mesoporous nature of the sample is further confirmed by its average pore diameter, which lies within the typical range for mesoporous materials.

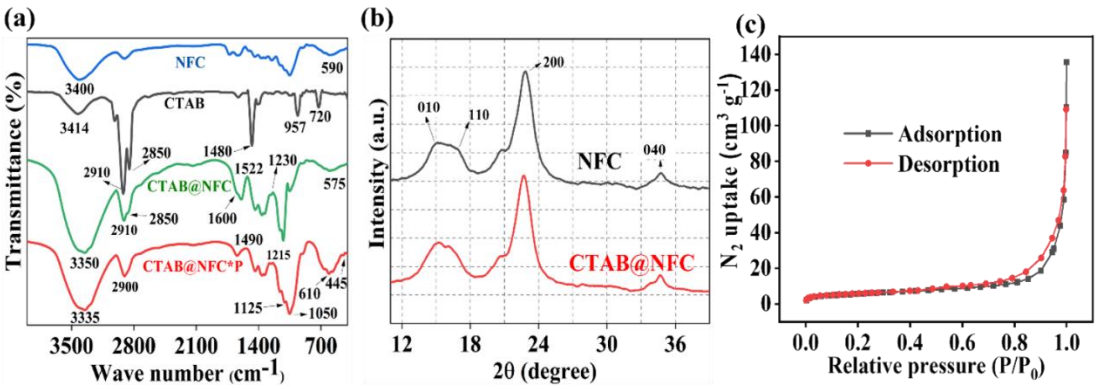

Figure 4.4 FT-IR spectra of (a) pristine NFC, CTAB, CTAB@NFC (before and after adsorption); (b) XRD patterns of pristine NFC and CTAB@NFC; (c) BET analysis of CTAB@NFC.

Table 4.1 BET specific surface area, average pore diameter, and total pore volume of synthesized CTAB@NFC.

Parameters	Results
Specific surface area (m^2/g)	60.2
Average pore diameter (nm)	18.7
Total pore volume (cc/g)	0.09

4.3.2 Effect of CTAB concentration on phosphate adsorption (pre-screen adsorption studies)

The preliminary assessment compared all the adsorbents to determine the optimal CTAB concentration for maximum phosphate adsorption (Figure 4.6 a). Additionally, for each pre-screening adsorption test, parallel experiments using pristine NFC and CTAB were also measured to contrast their adsorption efficiencies. The experiments revealed that the removal percentage for both pristine NFC and CTAB was significantly lower across all tested phosphate concentrations. NFC showed a removal efficiency of 28.5%, likely attributed to repulsion resulting from the negative charge of NFC surface [193]. In contrast, CTAB demonstrated a removal efficiency of only 16.2%, likely due to nonspecific interactions between CTA^+ (cetyltrimethylammonium) cations and phosphate anions driven by electrostatic attraction. The effect of concentration of CTAB for modification of NFC significantly influences the sorption of anions including phosphate. The figure illustrates the phosphate removal percentage and equilibrium adsorption capacities of NFCs quaternized with varying molar concentration of CTAB. Increasing the molar concentration of CTAB from 0.5 mM to 1 mM corresponded to an increase in phosphate removal percentage up to 85% and an adsorption capacity of 21.7 mg/g. Beyond this threshold, the adsorption capacity of the adsorbent remained relatively stable despite increasing the molar concentration of CTAB. This behaviour is ascribed to alterations in the gross surface charge density of modified NFCs.

When 0.5 mM of CTAB is introduced to the NFC suspension, CTA^+ cations adhere onto the surface of NFCs, accompanied by their cationic headgroups orienting towards the particles, as illustrated in Figure 4.5 (i). This change is driven by the electrostatic

attraction between the positively charged headgroups of the CTA^+ cations and the negatively charged OH^- groups on the NFC particle surface [202]. Consequently, the overall surface charge of the adsorbent ($CTAB_{0.5}$@NFC) becomes neutral, resulting in moderate adsorption capacity. Further increasing the CTAB concentration triggers the formation of admicelles on NFC surface (igure 4.5 (ii)), due to hydrophobic interaction between the hydrophobic tails of both bound and free surfactant molecules [213]. As a result, reversal of surface charge takes place, and the adsorbent ($CTAB_{1.0}$@NFC) acquires positive charge. This attributes to increase in adsorption capacity of $CTAB_{1.0}$@NFC_as demonstrated in Figure 4.6 a. However, at concentration slightly above the critical micelle concentration (CMC) of CTAB (1 mM), the NFC surface saturates with surfactant molecules, and supplemental addition of surfactant induces the formation of free micelles above the critical concentration [214] (Figure 4.5 (iii)) and fails to contribute to alter the overall surface charge of the material. This can be evidenced by the plateau observed in removal percentage of phosphate beyond CTAB CMC (≥ 1mM) (Figure 4.6 a). Based on these results, all subsequent experiments are conducted using $CTAB_{1.0}$@NFC as adsorbent.

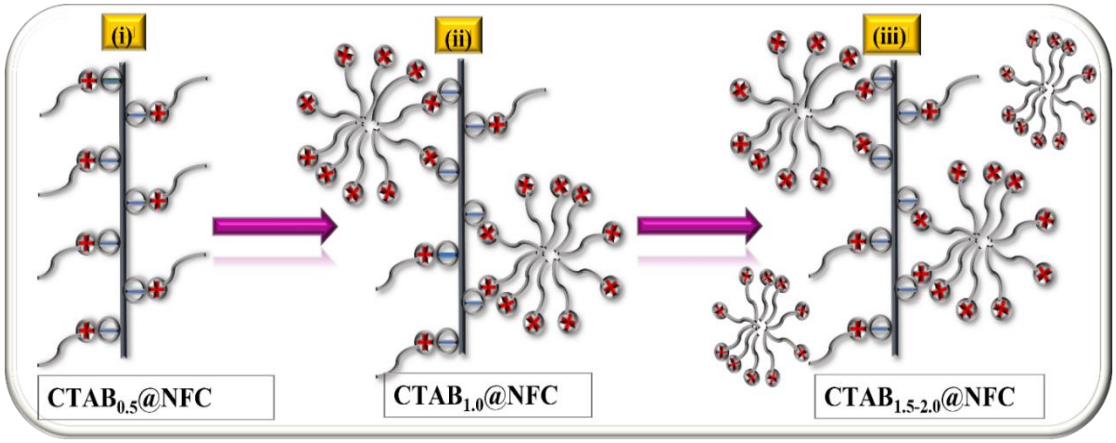

Figure 4.5 Schematic illustration of the interactions between CTAB and NFC at varying molar concentrations (0.5, 1, 1.5 and 2 mM).

4.3.3 Batch adsorption studies

4.3.3.1 Effect of adsorbent dose

Figure 4.6 b demonstrates an increased phosphate removal percentage from 38.8 % to 87.3 % with the increase in dose of CTAB@NFC from 0.5 to 2.5 g/L. This can be attributed to the ample number of binding sites on the adsorbent's surfaces. However, upon increasing adsorbent dose while maintaining fixed volume and initial phosphate concentration leads to insufficient utilization of active sites, causing the equilibrium adsorption capacity to decline from 32.2 to 16.88 mg/g. Also, at a specific concentration, using excess adsorbent can cause accumulation of the adsorbent resulting in minimal exposed surface area and decrease in the adsorption capacity [215]. Consequently, a dose of 2 g/L was determined to be optimal considering both cost-effectiveness and performance.

4.3.3.2 Effect of initial solution pH

The influence of pH on phosphate removal by CTAB@NFC was studied in details at pH values ranging from 3 to 11 and the obtained results are shown in Figure 4.6 e. As demonstrated in the figure, the quaternized NFC displayed remarkable phosphate removal performance at lower pH values, but exhibited a prominent decline in adsorption efficacy in elevated solution pH value. However, the adsorption capacity of the adsorbent increased only after pH 3 and subsequently sustained effective and steady removal within the pH range of 4–7. Conversely, a consistent decline in adsorption capacity was observed in solutions with pH values exceeding 7. At pH 4, the maximum adsorption capacity for phosphate reached 24.8 mg/g while at pH 9, the adsorption capacity dropped to a minimum of 13.77 mg/g, reflecting a decrease of 31.02 %.

Various factors may have affected this phenomenon. For instance, the surface charge of adsorbent contributes a pivotal role in the adsorption processes of both anions and cations as the introduction of positively charged quaternary ammonium groups in CTAB@NFC increased its zeta potential value to maximum of +22 mV (Figure 4.6 c) leading to enhanced removal capacity [216]. The point of zero charge (pH_{PZC}) of the adsorbent was pH 8.5 as shown in Figure 4.6 d. At pH levels below 8.5, the surface of the adsorbent becomes protonated, that exhibited positive electrical properties and enhanced electrostatic attraction with phosphate anions existing in solution [217]. This results in increased phosphate adsorption onto the adsorbent. Conversely, at higher pH levels ($\geq$ 8.5), the adsorbent's surface becomes electronegative, resulting in electrostatic repulsion and thus reducing its effectiveness for phosphate adsorption [218]. However, post sorption, the pH of the solution gradually increased that suggests that using CTAB@NFC to adsorb phosphate can enhance the solution's alkalinity, potentially helping to address water acidity issues. Additionally, the PZC of the CTAB@NFC adsorbent post adsorption shifted to 6.89, indicating a significant decrease from its initial value. This change can be attributed to surface charge neutralization due to site protonation occurring near the surfactant-loaded surface within the shear plane [219]. The next factor influencing adsorption capacity of adsorbent was the presence of varied configurations of phosphate at various pH levels. Below pH 3, H_3PO_4 is the dominant species that is unfavourable for adsorption process. The increase in adsorption capacity between pH 3 and 7, can be explained by the sequential shift from poorly adsorbed H_3PO_4 to strongly adsorbed $H_2PO_4^-$. And between pH 7 and 12, the predominant species is HPO_4^{2-} [220]. Thus, it is evident that in general, pH values substantially affect the phosphate species existing in solution and significantly influence the adsorption

processes. The third aspect that caused a decrease in adsorption capacity is due to competition between phosphate anions and the plentiful hydroxyl anions present in alkaline solutions. This phenomenon indicates that ligand exchange between phosphate and hydroxyl ions on CTAB@NFC surface is a key factor in phosphate adsorption [217]. Thus, the experimental findings suggests that the developed adsorbent in this study showed appreciable removal of phosphate at weakly acidic or neutral pH conditions, thereby streamlining the treatment process by reducing the need for significant pH adjustment.

4.3.3.3 Effect of interfering anions on phosphate removal

Real wastewater contains abundant other anions that undoubtedly compete with phosphate ions for the CTAB@NFC binding sites. To address this, the phosphate removal efficiency of CTAB@NFC was evaluated in the presence of co-existing anions such as Cl^-, NO_3^-, HCO_3^- and F^- at molar ratios corresponding typical wastewaters to different concentrations of phosphate (20 mg/L and 40 mg/L). The adsorption results (Figure 6 f) showed that multivalent phosphate anions were adsorbed more effectively than monovalent anions. This difference is likely due to the different charge states of these anions [193]. It can be seen that the effect of Cl^- and NO_3^- on phosphate removal percentage was negligible and could be undervalued. This could be possibly due to the lesser affinity of these anions, as they only form unstable complexes with adsorbent's surfaces. Contrastingly, among the various anions, HCO_3^- ions had the most significant impact, decreasing the phosphate removal percentage by 30.33%. This effect can be attributed to the dissolution of $NaHCO_3$, a weak acid salt, which increases the pH of solution. Consequently, the positive charges on the adsorbent surface decrease, directly reducing the electrostatic attraction between phosphate and CTAB@NFC [221]. In

comparison to the control group, fluoride ions at both low and high concentrations also exhibited a noticeable inhibitory effect on phosphate adsorption. The removal efficiency was 53.7 % at low concentration and 59.09 % at high concentration, compared to 82.37 % and 67.9 % respectively in the control group. This suggests a specific competitive adsorption mechanism influenced by the radius of fluoride ions [217]. Despite the obvious effects of coexisting anions, the experimental results demonstrated that the engineered adsorbent developed in this study remains highly effective in reclaiming phosphate from wastewater, especially under conditions of low phosphate anion concentration.

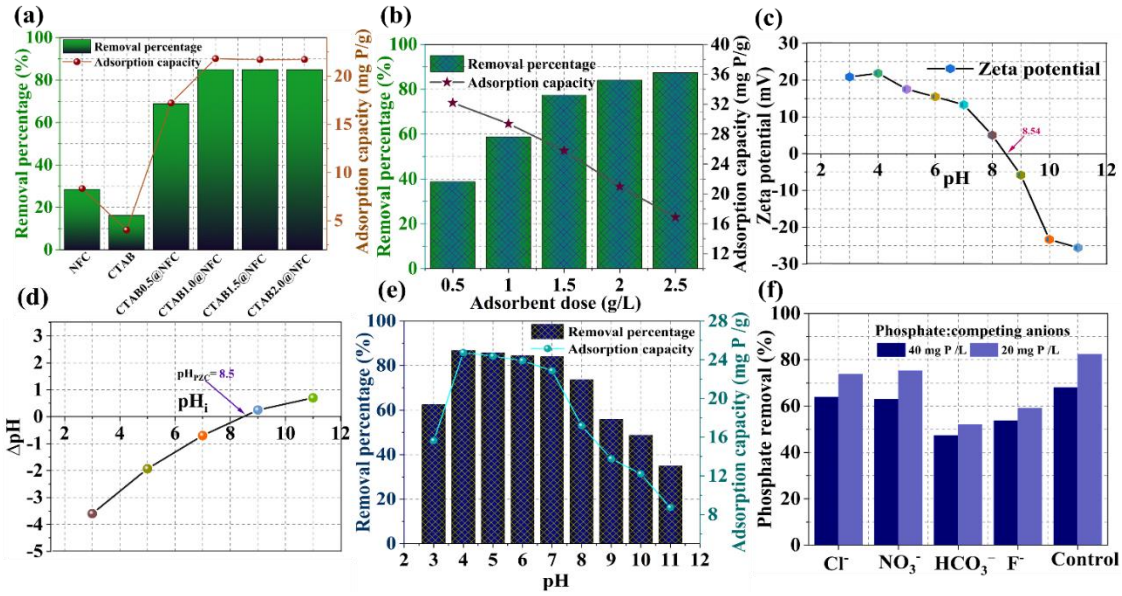

Figure 4.6 (a) Pre-screen adsorption of pristine NFC, CTAB, NFC modified with CTAB at varying molar concentrations (0.5, 1, 1.5 and 2 mM); (b) effect of adsorbent dose (0.5-2.5 g/L) on phosphate removal by CTAB@NFC (initial conc. 20 mg/L, initial pH 7.0 ± 0.2, contact time 2h); (c) zeta potential value and; (d) pH_{PZC} value of CTAB@NFC respectively; (e) effect of different pH values (3-11) on phosphate removal (initial conc. 20mg/L, dose 2 g/L, contact time 2h); (f) effect of competing anions (initial conc. 20/40 mg/L, dose 2 g/L, initial pH 7.0 ± 0.2, contact time 2h), the concentration of interfering anions correspond to typical wastewaters reported in literature.

4.3.3.4 Effect of contact time and kinetic studies

Figure 4.7 a depicts the mass transfer performance of CTAB@NFC, evaluated over different contact time. The study demonstrated that the adsorption of phosphate was quite rapid within the first 30 minutes. However, the rate decreased thereafter as the leftover vacant sites became sterically hindered by the already bound phosphate molecules. This process continued until it attained equilibrium concentration at around 22 mg/g in 120 minutes. This can be attributed by; (i) the numerous saturated adsorption sites on the surface of CTAB@NFC and, (ii) an eventual decrease in the concentration gradient between the bulk solution and adsorbent [222,223]. The experimental data were further modelled by Pseudo-first-order (PFO), Pseudo-second-order (PSO), and Elovich models without linearizing transform (Figure 4.7 b). According to the parameters in Table 4.2, the q_e calculated value derived from the pseudo-second-order model aligns well with experimental q_e value. Moreover, the R^2 value from the pseudo-second-order model significantly exceeds that of the pseudo-first-order model and the Elovich model ($R^2 > 0.99$). This indicates that chemisorption is the main mechanism, although detailed adsorption mechanisms could be further investigated using XPS analysis [219].

4.3.3.5 Effect of initial phosphate concentration and isotherm studies

To examine the impact of varying phosphate concentrations on the removal efficiency of phosphate by CTAB@NFC in an aqueous solution, experiments were conducted with the following fixed parameters: a contact time of 2h, adsorbent dose of 0.1g, and a test solution volume of 50 mL with different initial phosphate concentrations varying from 5 mg/L to 40 mg/L. As seen in Figure 4.7 c, the highest removal percentage, 87.7%,

was achieved with an initial phosphate concentration of 10 mg/L, whereas a removal efficiency of 84.72 % was recorded with a phosphate concentration of 20 mg/L. However, concentration of 20 mg/L was chosen for experimentation as the typical phosphate levels found in municipal wastewater lies within this limit. Figure 4.7 d presents the phosphate adsorption isothermal curves of CTAB@NFC, and the best-fit parameters are shown in Table 4.3. The R^2 value exceeding 0.9 for all three isotherm models demonstrates a good fit. Nevertheless, when accounting to additional decimal places precisely, the models can be arranged as follows: Sips > Langmuir > Freundlich. Notably, both Langmuir and Sips isotherm models show exceptionally strong fit, with R^2 value of 0.978 and 0.989 respectively (as presented in Table 4.3) aligning more closely with the experimental data, suggesting that the interaction between phosphate and adsorbent is influenced by both Langmuir and Freundlich processes. These findings are in line with the kinetic data and indicates that the sorption of phosphate is governed by multiple mechanisms. Therefore, the adsorption behaviour cannot be entirely described by a single isotherm model, and that both models contribute to the overall adsorption process [221].

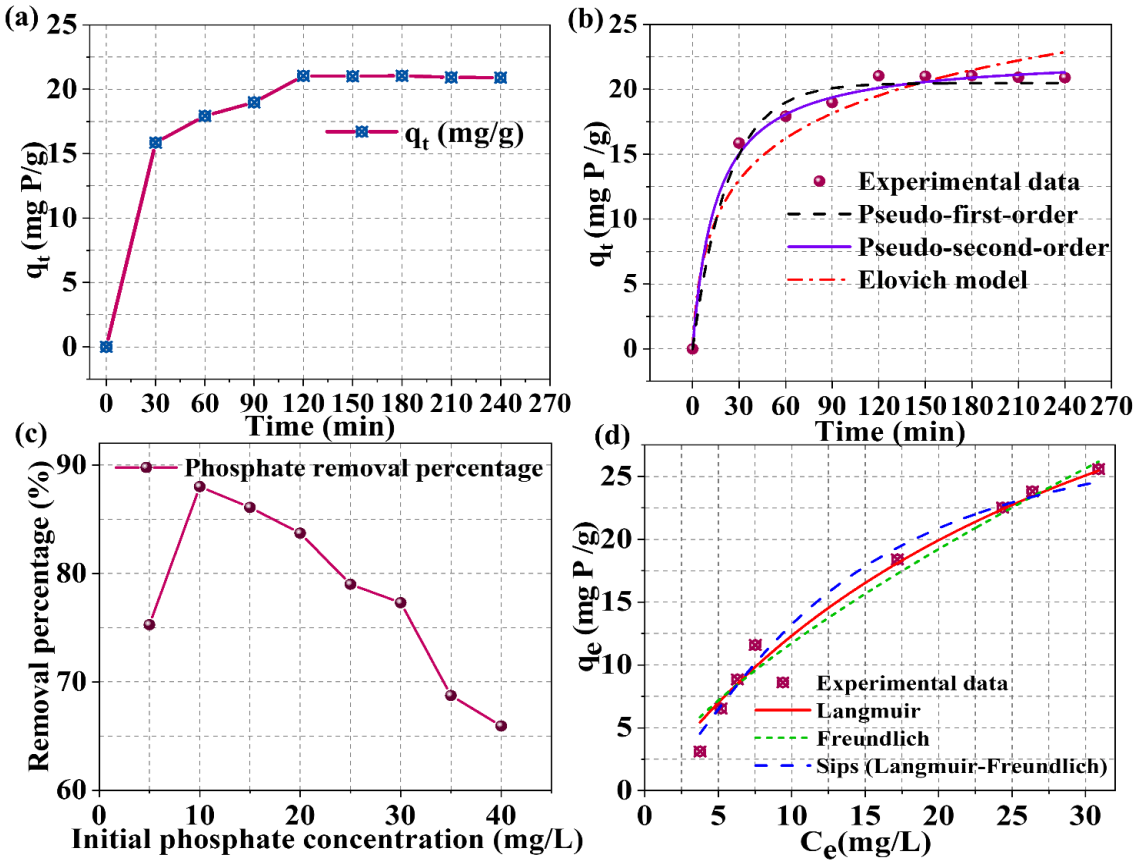

Figure 4.7 (a & b) Effect of different contact time (0-240 min) on phosphate removal by CTAB@NFC and adsorption kinetics (at ambient temperature, initial conc. 20mg/L, dose 2 g/L, initial pH 7.0 ± 0.2); (c & d) Effect of different initial concentration (5-40 mg/L) on phosphate removal by CTAB@NFC and adsorption isotherm (at ambient temperature, dose 2 g/L, initial pH 7.0 ± 0.2, contact time 2h); the points and lines depict the experimental data and fitting curves of kinetic and isotherm models, respectively.

Table 4.2 Adsorption kinetic parameters of phosphate removal on CTAB@NFC.

Models	Parameters	CTAB@NFC
Pseudo-first-order kinetic model	q_e (mg/g)	20.48 ± 0.02
	k_1 (min^{-1})	0.04
	R^2	0.96
Pseudo-second-order kinetic model	q_e (mg/g)	22.66 ± 0.04
	k_2 (g/mg/min)	0.02
	R^2	0.99
Elovich model	α (mg/g/min)	2.16
	β (g/mg)	0.20
	R^2	0.92

Table 4.3 Adsorption isotherm parameters of phosphate removal on CTAB@NFC.

Models	Parameters	CTAB@NFC
Langmuir	Q_0 (mg/g)	52.004
	K_L (L/mg)	0.03
	R^2	0.97
Freundlich	n_F	1.40
	K_F (mg/g)(L/mg)$^{(1/n)}$	2.28
	R^2	0.96
Sips	q_m (mg/g)	30.35
	K_S (L/mg)^n	0.023
	n_S	1.21
	R^2	0.99

4.4 Possible mechanism of phosphate removal on CTAB@NFC

FTIR and XPS analysis can help to comprehensively investigate the phosphate adsorption mechanism using CTAB@NFC. FTIR analysis of CTAB@NFC before and after adsorption revealed that quaternary ammonium groups were effectively grafted onto the NFC surface. The alteration in the band for the alkyl group of the quaternary nitrogen at 1480 cm^{-1} indicates the involvement of CTA^+ groups in the adsorption process, suggesting that phosphate ions were adsorbed onto the CTAB@NFC surface through electrostatic attraction between negatively charged phosphate ions and positively charged quaternary ammonium (CH_3-N^+) groups.

XPS was employed to quantitatively analyse the element composition and further comprehend the interactions between CTAB-modified NFC and phosphate. As illustrated in Figure 4.8 d, the survey spectra verified that the newly synthesized adsorbent consisted of C, O, N and Br aligning with the EDX findings. As seen in Figure 4.8 c, the XPS survey spectrum displays a new peak for P 2p at 133.2 eV, suggesting surface adsorption of phosphate ions on to the adsorbent [224]. Considering the role of positively charged CTA^+ ions, the peak-split of C1s and N1s was performed to evaluate the associated bonding types and gain deeper insight into the underlying adsorption mechanism. The high-resolution XPS peak for C 1s provides information

about the chemical environment of quaternized NFC. Figure 4.8 a show the deconvolutions of the C 1s for CTAB@NFC before and after adsorption. C 1s spectrum includes four component types; C1: C-C, C-H, C2: C-O, C2': C-N and C3: C–OH / C–O–C. The peak at 284.4 eV, attributed to the C-N bond of the quaternary ammonium group upshifted due to the involvement of this group in the adsorption process. Additionally, following phosphate adsorption, the distinctive peak of C–OH / C–O–C shifted to a higher binding energy of 287 eV, and the peak area decreased by 27.2%. This suggests possible hydrogen bonding between the hydrogen atom on phosphate and the cellulose (OH) groups, forming P-O-H… HO–C/C–O–C [225]. The peaks at C1 and C2 showed minimal change, indicating that C-C/C-H and C-O are not the primary active sites for phosphate uptake.

N 1s spectra of CTAB@NFC displayed two peaks: one at 398.9 eV corresponding to aliphatic N-C and another at 401.75 eV for $-N^{+}(CH_3)_3$ (quaternary N), is in agreement to FTIR results [226] (Figure 4.8 b). These prominent peaks indicate that the surface of NFC was effectively modified by cationic surfactant CTAB, demonstrating that NFC possesses flexible surface functionality properties. Obviously, the intensity of quaternary–N peak is much stronger than that of aliphatic N–C peak as seen in the figure. However, the content of quaternary-N decreased from 66.7% to 49% and showed slight shift towards higher energy after adsorption process, manifesting that the overall interaction between trimethylammonium and phosphate is primarily driven by electrostatic attraction due to the positive charge of trimethylammonium ions and negative charge of phosphate ions [194]. This can be described as a Lewis acid-base interaction where the anionic $H_2PO_4^-$ acts as an electron donor and trimethylammonium acts as an electron acceptor [227]. The increase in the intensity of the aliphatic N-C peak after adsorption may indicate altered state of CTAB on the surface, likely due to interactions or structural changes induced by the phosphate ions.

4.5 Stability of adsorbent

Desorption refers to the process where molecules that were previously attached to a surface are released [228]. This method serves as an index to assess the adsorption stability of the prepared adsorbent. Three desorption tests were performed on CTAB@NFC that had adsorbed phosphate, with the results displayed in Figure 4.8 e. It was observed that the phosphate desorption percentage was relatively high during the first cycle and decreased progressively in subsequent cycles. The total desorption percentage across all three cycles was 12.61%. Overall, CTAB@NFC demonstrated excellent phosphate retention capacity, suggesting that the adsorbent is highly effective at retaining phosphate, and the phosphate can be bound to the adsorbent through chemical adsorption.

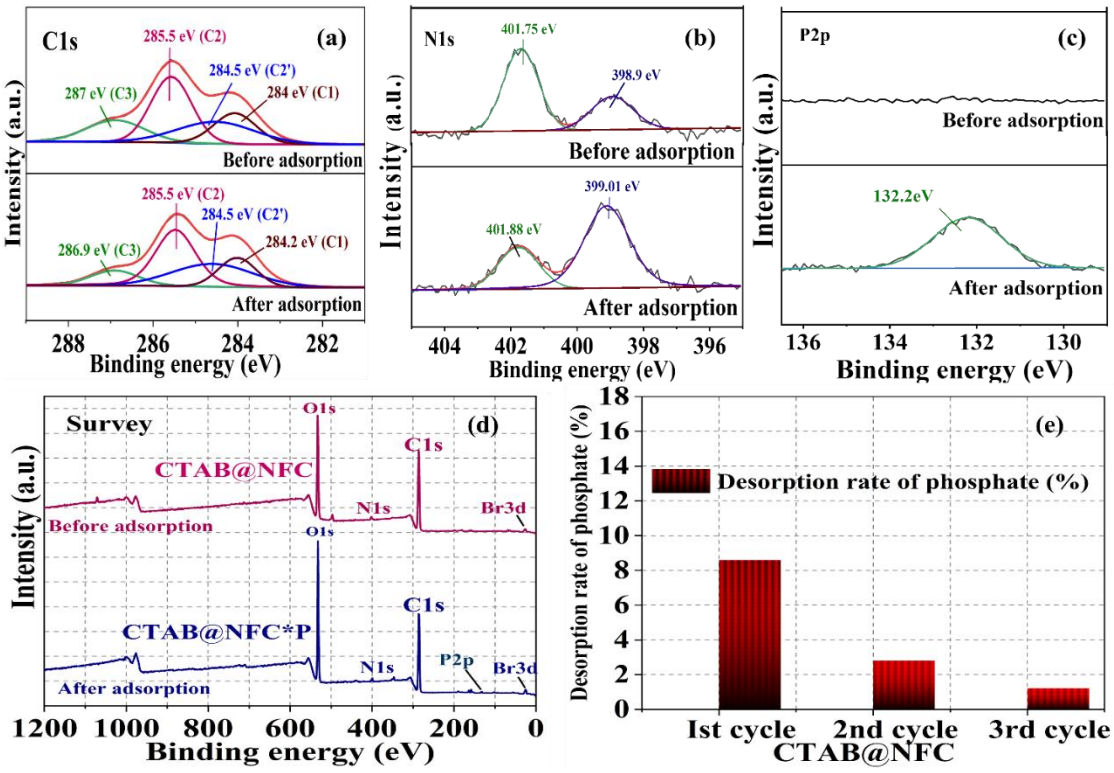

Figure 4.8 XPS spectra of CTAB@NFC prior to and post phosphate adsorption: (a) C 1s spectra; (b) N 1s spectra; (c) P 2p spectra; and (d) survey scanning spectra of adsorbents (pre- and post-adsorption); (e) desorption rate of phosphate on CTAB@NFC.

In summary, the mechanisms of phosphate removal by CTAB@NFC can be outlined as follows: (i) the presence of N-containing groups introduced by CTA^+ decoration leads to electrostatic attraction based on the Lewis acid-base principle at pH values below the pH_{PZC}, and (ii) protonated phosphate anions could form hydrogen bonds with H-bond acceptors (O=C). Figure 4.9 depicts the proposed mechanism for phosphate removal by CTAB@NFC, derived from adsorption performance and characterization analyses.

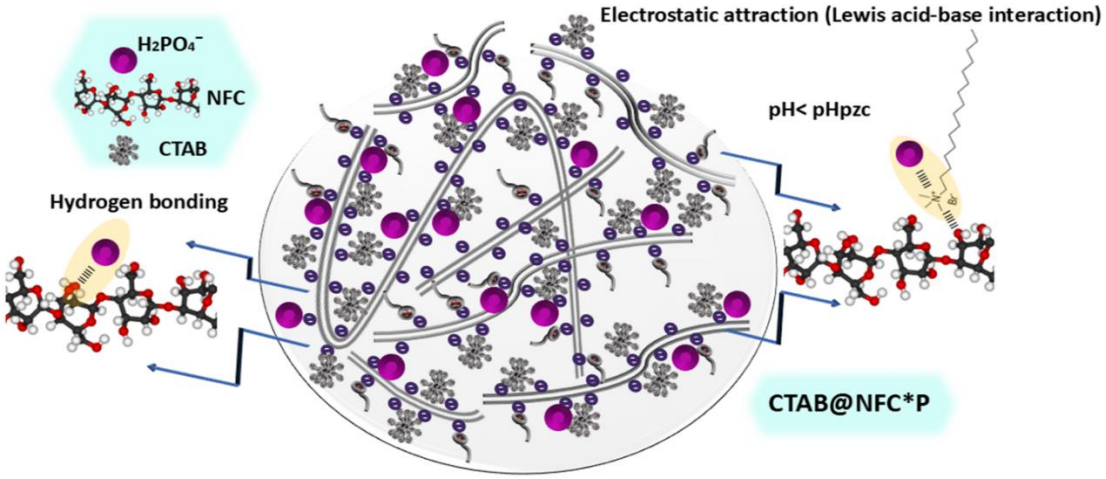

Figure 4.9 Representation of possible adsorption mechanisms for phosphate removal on CTAB@NFC.

4.6 Conclusions

In this work, we prepared a highly efficient and low-cost adsorbent for phosphate uptake using agro-waste derived biomacromolecule, nanofibrillated cellulose. Through a facile quaternization technique, cationic NFC adsorbent was synthesized using CTAB. The influence of important factors such as dose, pH, contact time, initial concentration, and effect of interfering anions are systematically investigated along with adsorbent's stability. CTAB@NFC resulted a maximum adsorption capacity of 21.78 mg/g and best fits in Sips isotherm model and the kinetic data aligns well with

pseudo-second-order model. The underlying adsorption mechanisms have been elucidated as hydrogen bonding and electrostatic attraction. The phosphate-loaded adsorbent also exhibits remarkable stability in an aqueous environment across three consecutive cycles. Concluding that, this study paves way for promising future research, as CTAB-modified NFCs, following desorption, could also be utilized in antimicrobial assays due to intrinsic antibacterial and antifungal properties of CTAB. Additionally, investigating various strategies for modifying NFCs with sustainable and greener surfactants to enhance their capacity for removing phosphate anion or other anions from wastewater presents valuable prospects for research focused on advancing environmental sustainability.